THE JOURNAL OF PHYSICAL CHEMISTRY A

ARTICLE

pubs.acs.org/JPCA

Reaction of HOD^+ with NO_2: Effects of OD and OH Stretching, Bending, and Collision Energy on Reactions on the Singlet and Triplet Potential Surfaces

Jason M. Boyle, David M. Bell, and Scott L. Anderson*

Chemistry Department, University of Utah, 315 South, 1400 East Room 2020, Salt Lake City, Utah 84112, United States

A. A. Viggiano

Space Vehicles Directorate, Air Force Research Laboratory, Hanscom Air Force Base, 29 Randolph Road, Massachusetts 01731-3010, United States

ABSTRACT: Integral cross sections and product recoil velocity distributions were measured for the reaction of HOD^+ with NO_2, in which the HOD^+ reactant was prepared in its ground state and with mode-selective excitation in the 001 (OH stretch), 100 (OD stretch), and 010 (bend) modes. In addition, we measured the 300 K thermal kinetics in a selected ion flow tube reactor and report product branching ratios different from previous measurements. Reaction is found to occur on both the singlet and triplet surfaces with near-unit efficiency. At 300 K, the product branching indicates that triplet → singlet transitions occur in about 60% of triplet-coupled collisions, which we attribute to long interaction times mediated by complexes on the triplet surface. Because the collision times are much shorter in the beam experiments, the product distributions show no signs of such transitions. The dominant product on the singlet surface is charge transfer. Reactions on the triplet surface lead to NO^+, NO_2H^+, and NO_2D^+. There is also charge transfer, producing NO_2^+ (a^3B_2); however, this triplet NO_2^+ mostly predissociates. The NO_2H^+/NO_2D^+ cross sections peak at low collision energies and are insignificant above ~1 eV due to OH/OD loss from the nascent product ions. The effects of HOD^+ vibration are mode-specific. Vibration inhibits charge transfer, with the largest effect from the bend. The NO_2H^+/NO_2D^+ channels are also vibrationally inhibited, and the mode dependence reveals how energy in different reactant modes couples to the internal energy of the product ions.

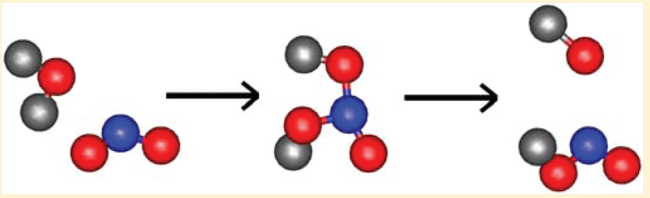

I. INTRODUCTION

Water with a single deuterium label, HOD, is interesting from a vibrational dynamics perspective because the 100 mode has primarily OD stretching character, the 001 mode primarily involves OH stretching, and the 010 mode (the bend) involves yet another distinct type of motion. This fact was exploited in studies of H- versus D-transfer reactions of HOD with hot H atoms[1−6] and with Cl atoms.[7] Reaction of HOD excited to the fourth overtone of the OH stretch or to the nearly isoenergetic fifth overtone of the OD stretch showed a strong propensity to break the excited bond.[8] Zare and co-workers showed that even for excitation of the fundamental of these modes, there were dramatic shifts in the OH versus OD product branching, again strongly favoring breaking the excited bond.[3] Vibrational energy was found to be ~120 times more effective at driving reaction than equal amounts of collision energy. Furthermore, the initial mode of excitation had a strong effect on how energy was partitioned to internal states of the product. For example, in the Zare experiments on HOD + Cl, fundamental OH stretch excitation lead 73% of the available energy partitioned to the HCl stretch, leaving the OD spectator bond in its vibrational ground state.[5] Similarly, in the study of OD-stretch-excited HOD reacting with hot H atoms, the OH products were exclusively produced in $v = 0$, while OD products were formed in $v = 1$, that is, the reaction preserved the excitation level in the spectator bonds.

The effects of bond-specific excitation in neutral−neutral collisions mostly result from the effects of the excitation upon crossing the rather substantial barriers to reaction. In most ion−molecule reactions, attractive electrostatic interactions and the stabilization that results from charge delocalization in the collision complex tend to reduce the energy in the region of the potential surface where bonds are being broken and made and therefore tend to reduce or eliminate barriers to reaction. As a result, it is not obvious what to expect in the way of mode- or bond-specific vibrational effects. Here, we present a study of the reaction of HOD^+ with NO_2, chosen because in this system, H^+ and D^+ transfer are essentially thermoneutral. Furthermore, the

Received: November 3, 2010
Revised: December 29, 2010
Published: February 3, 2011

resulting NO_2H^+ and NO_2D^+ products have low-energy OH or OD loss channels, and this secondary dissociation process provides a built-in "thermometer" that allows us to monitor how energy initially in the bond that breaks, versus the spectator bond, is partitioned to the internal energy of the products.

When a pair of doublet spin molecules like HOD^+ and NO_2 collide, one-quarter of the collisions will occur with singlet coupling of the unpaired electrons on the two reactants, and three-quarters of collisions will occur with triplet coupling. In many systems, such triplet-coupled collisions are unreactive or even repulsive because the unpaired electrons are unable to form bonds.[9] One question of interest for this system, therefore, is the extent to which reaction occurs on the triplet surface. Another point of interest is the possibility for singlet ↔ triplet transitions during collisions. Because there are no heavy atoms with large spin−orbit coupling constants, the singlet ↔ triplet transition rate should be slow; however, if the collision times are long enough, transitions may be significant. This issue is addressed below by comparing product branching in thermal kinetic and beam measurements, probing collisions over time scales that vary by orders of magnitude, and, therefore, providing insight into the time scale for such spin-forbidden processes.

The thermal energy kinetics of H_2O^+ with NO_2 were previously studied in both flow-drift tube (FDT)[10] and selected ion flow tube (SIFT)[11] configurations at 300 K, and both studies reported a rate constant of 1.2×10^{-9} $cm^3/mol \cdot s$, corresponding to essentially unit reaction efficiency. The reported branching was 100% to the NO_2^+ product of charge transfer (CT). There are several surprising aspects of this result. CT can only produce singlet products at thermal energies because the triplet CT channel is endoergic. Therefore, the 100% NO_2^+ branching implies that all collisions starting with triplet coupling end up on the singlet surface, even though there are exothermic triplet reactions producing NO^+ and $NO^+(H_2O)$ that should be quite efficient. The absence of signal for these triplet product channels would seem to imply that they have significant barriers, as well as require unusually strong singlet−triplet coupling.

To provide further insight into these issues, we present a combined thermal energy and beam study of this system. We report integral cross sections and product recoil velocity distributions for reaction of HOD^+ with NO_2, in which the HOD^+ reactant was prepared in its ground state and with mode-selective excitation in the 001 (predominantly OH stretch), 100 (predominantly OD stretch), and 010 (bend) modes, as discussed in the next section. In addition, we remeasured the 300 K kinetics in a SIFT apparatus, with careful attention to extracting branching ratios.

II. EXPERIMENTAL AND COMPUTATIONAL METHODS

A. State-Selected Beam Experiments. The cross section measurements were made in a guided ion beam instrument at the University of Utah, described in detail previously,[12,13] along with our calibration and data analysis procedures. HOD^+ is produced in its ground state or with one quantum of bend (010 = 153 meV), OD stretch (100 = 293 meV), or OH stretch (001 = 397 meV) excitation by 2 + 1 REMPI through the C $^1B_1$ state.[14] In that study, photoelectron spectroscopy was used to measure the resulting ion state purity, which is essentially 100% for HOD^+ in its ground state and with one quantum of either OD or OH stretch excitation. When preparing bend-excited HOD^+, however, ~56% of the ions are in the desired state, with 44% in the ground state. Because we measure cross sections for the ground-state reaction, the cross sections for bend excitation can be obtained by subtraction, which has been done for all of the results below.

For these experiments, helium was bubbled through a room-temperature $H_2O/HOD/D_2O$ mixture, producing ~4% water/He that was pulsed into the experiment as a supersonic beam and then collimated by a skimmer before passing into the ionization region. Ionization occurred between a pair of planar electrodes, and the resulting ions were then injected into a quadrupole ion guide, which focused them into a quadrupole mass filter to remove any fragment and unwanted isotope ions produced in the REMPI process. At the end of the mass filter, a time-of-flight (TOF) gate was used to narrow the kinetic energy spread of the reactant ion beam. The state-, mass-, and energy-selected ions were injected into the first section of an eight-pole ion guide and passed through a scattering cell containing 0.1 mTorr of NO_2. Product ions, together with unreacted H_2O^+, were contained within the guide and passed into a second, longer guide section for TOF velocity analysis. Product ions that were backscattered in the laboratory frame were reflected at the entrance of the guide by a positive potential on the injection lens, so that they could be detected. Finally, the ions were mass analyzed and counted using a P7882 FAST ComTec multichannel scalar. The experiment was controlled by a LabView program that cycles through collision energies and masses of interest and switches the target gas flow between the scattering cell and chamber background and accumulates TOF data for reactant and product ions at each energy. Integral cross sections were calculated from the ratio of reactant and product ion intensities, corrected for ions formed outside of the scattering cell, using the calibrated effective length of the scattering cell[12] and the pressure, measured with a capacitance manometer, which was checked against an ionization gauge.

TOF was used both to measure the energy distribution of the reactant ion beam and the axial projection of the recoil velocity distribution for the product ions (v_{axial}). The reactant ion velocity distributions at each E_{col} could be fit within experimental error to Gaussians, defining the absolute energy and energy spread (<150 meV for all E_{col}) of the beam. TOF data were collected for product ions at a series of collision energies and for each vibrational state. Several complete sets of cross sections for the four reactant states and three product channels were recorded as a function of collision energy (E_{col}), each taking several days because the ion beam intensity obtainable by REMPI is relatively low (~1200 ions/s). To avoid systematic errors comparing different vibrational states, the ground-state cross sections were collected every day as a check on possible changes in instrument conditions. If the ground-state cross section was found to differ from the average by more than 10%, the entire day's data was discarded. On the basis of the variations from set to set, we estimate that the relative error in comparing cross sections for different vibrational states or collision energies is <15%, including statistical and systematic errors. The exception is that for the weak NO_2H^+ and NO_2D^+ channels, particularly at high E_{col}, the statistical error is larger and can be judged from the scatter in the data. We estimate the uncertainty in the absolute cross section to be about 20% due to possible mass-dependent detection efficiency in the final mass spectrometer.

We considered the possibility that the NO_2 in the scattering cell might be contaminated by either NO or N_2O_4, which is in equilibrium with NO_2. If either contaminant were present at concentrations greater than a few percent, there would be significant contributions to the NO^+ and possibly NO_2^+ product signals. Mass analysis of $NO/NO_2/N_2O_4$ mixtures is ambiguous because of fragmentation that is quite sensitive to small changes in ionization conditions. The presence of significant NO was ruled out by running a gas-phase IR spectrum of the NO_2 at high enough pressure that the weak symmetric stretch transition for NO_2 was nearly saturated. No signal was seen for the much stronger NO stretch transition. The equilibrium concentration of N_2O_4 at the 10^{-4} Torr of pressure in our scattering cell is negligible,[15] but we had some concern that the time constant for reaching equilibrium[16] might leave some undissociated N_2O_4. This possibility was tested by measuring cross sections using NO_2 supplied from reservoirs at atmospheric pressure and at ~50 Torr, where the equilibrium N_2O_4 concentration is 13 and 1%, respectively. No change in product cross sections was observed; thus, we conclude that both NO and N_2O_4 contaminants are negligible under our conditions.

B. Selected Ion Flow Tube (SIFT) Measurements. The measurements of the 300 K kinetics were performed using the Air Force Research Laboratory's SIFT. The details of the instrument have been described previously,[17] and only information important to the specific experiments is reported here. H_2O^+ is generated by electron impact from water vapor. While we could selectively inject the desired ion into the flow tube, H_2O and O_2 impurities in the helium buffer gas created H_3O^+ (~30%) and O_2^+(~10%) in the flow. Therefore, we studied these reactions under the same conditions and subtracted their influence from the product distributions. H_3O^+ was essentially nonreactive. The O_2^+ experiment showed that the NO_2 (1% in helium) had a small NO impurity (2−4%). This was easy to correct for because H_2O^+ reacting with NO produces only NO^+. Product branching was measured under low depletion conditions so that little secondary reaction occurred. The net effect of the corrections was small, well within our reported uncertainty, a few percent.

C. Computational Methods. To construct the reaction coordinate shown in Figure 1, ab initio structure optimization calculations were performed at the PBE1PBE/6-311++G** level of theory using GAUSSIAN 03.[18] For all stable singlet structures and for the triplet products, the calculations were repeated at the G3 level, and for the singlet complexes and transition states, we also did single-point calculations at the QCISD(T)/cc-pVTZ level at the geometries optimized at the PBE1PBE/6-311++G** level. The energetic trends were consistent for the levels of theory and are reported in Table 1.

We also calculated a small set of quasi-classical trajectories to examine breakup of a covalently bound complex on the singlet reaction coordinate. The VENUS program of Hase and co-workers[19] was used to calculate the quasi-classical initial conditions, and direct dynamics trajectories were integrated at the B3LYP/6-31G* level using the updating Hessian method of Schlegel and co-workers,[20] implemented in GAUSSIAN03.[18]

III. RESULTS AND DISCUSSION

A. Reactions and Reaction Coordinate. Product ions are observed in the beam experiments at masses 46 (NO_2^+), 47 (NO_2H^+), 48 (NO_2D^+), and 30 (NO^+), with the corresponding energetics listed in Table 1. The experimental[21−24] energetics for all primary reactions that might lead to the observed product ions are

$H_2O^+ + NO_2 \rightarrow$	$NO_2H^+ + OH$	(H^+ transfer)	$\Delta H_{rxn}(0K) = -0.03$ eV
	$\downarrow$		
	$NO^+ + 2\,OH$	(2^{nd}ry dissoc. of NO_2H^+)	$\Delta H_{rxn}(0K) = +0.45$ eV
$\rightarrow$	$NO_2^+(^1\Sigma_g) + H_2O$	(singlet CT)	$\Delta H_{rxn}(0K) = -3.03$ eV
$\rightarrow$	$NO_2^+(a^3B_2) + H_2O$	(triplet CT)	$\Delta H_{rxn}(0K) = +0.17$ eV
	$\downarrow$		
	$NO^+ + O(^3P) + H_2O$	(sequential triplet dissoc. CT)	
$\rightarrow$	$NO^+ + O(^3P) + H_2O$	(concerted triplet dissoc. CT)	$\Delta H_{rxn}(0K) = -0.18$ eV
$\rightarrow$	$NO^+ + O(^1D) + H_2O$	(singlet dissoc. CT)	$\Delta H_{rxn}(0K) = +1.78$ eV
$\rightarrow$	$NO^+ + HOOH$	(O^- abstraction)	$\Delta H_{rxn}(0K) = -1.67$ eV
$\rightarrow$	$NO^+(H_2O) + O(^3P)$	(triplet O elimination)	$\Delta H_{rxn}(0K) = -0.82$ eV

The "sequential triplet dissociative CT" channel corresponds to CT to form NO_2^+ (a^3B_2), followed by predissociation to $NO^+ + O(^3P)$; thus, the effective barrier is the 0.17 eV endoergicity associated with forming NO_2^+ (a^3B_2). The value given for the final reaction listed was determined from a PBE1PBE/6-311++G** calculation (BSSE-corrected) for the stabilization energy of the $NO^+(H_2O)$ complex, referenced to the experimental energy for $NO^+ + O(^3P) + H_2O$.

For reaction of HOD^+, the energetics are slightly different due to the zero-point energy (ZPE). The only channel where the ZPE has a significant effect is H^+ versus D^+ transfer. Using the experimental exoergicity for H^+ transfer from H_2O and taking the reactant and product ZPEs from calculations at the B3LYP/6-311G(df,p) level, scaled by 1.0167,[25] we find

$$HOD^+ + NO_2 \rightarrow NO_2H^+ + OD \quad (H^+ \text{ transfer}) \quad \Delta H(0K) = -0.025 \text{ eV}$$

$$\rightarrow NO_2D^+ + OH \quad (D^+ \text{ transfer}) \quad \Delta H(0K) = -0.052 \text{ eV}$$

that is, both H^+ and D^+ transfer from HOD^+ to NO_2 are slightly exoergic, but ZPE favors D^+ transfer. It is not clear how important this ~27 meV difference in energetics for H^+ versus D^+ transfer might be, given that at our lowest E_{col}, the available energy, is an order of magnitude greater ($E_{col} + NO_2$ rotation ≈ 0.3 eV). We also calculated the density of states (DOS) in the two product channels in the low E_{col} range where they are significant. At our lowest E_{col}, the density of states is ~10% higher in the $NO_2H^+ + OD$ channel compared to that in $NO_2D^+ + OH$; thus, this factor might tend to compensate for the small difference in energetics.

Figure 1 shows the reaction coordinate assembled using experimental energetics[21,26,27] for reactants and products and energies calculated at the PBE1PBE/6-311++G** level for complexes and transition states, referenced to the calculated reactant energy. To simplify the diagram, the reaction coordinate is shown for H_2O, rather than HOD. Species and reaction coordinates that are singlets are shown in blue, triplet species and reaction coordinates are in red, and doublet species are in green. The H_2O^+ and NO_2 reactants are both doublets; therefore, collisions will occur in both singlet and triplet coupling, with a 1: 3 ratio. A flowing afterglow study[28] was reported for the

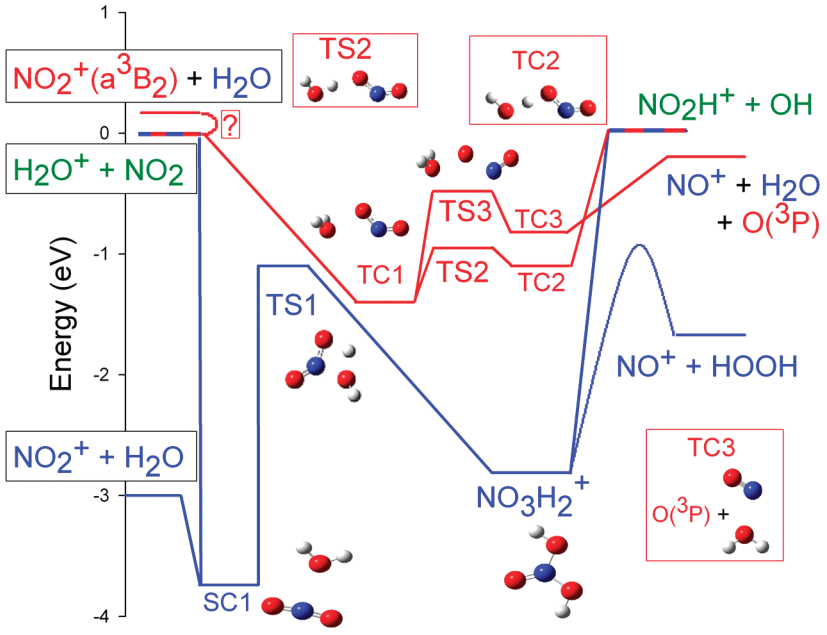

Figure 1. Reaction coordinate for the $H_2O^+ + NO_2$ system. Blue indicates species and reaction coordinates that are singlets, red indicates triplets, and green indicates doublets.

Table 1. Experimental and Ab Initio Energies (eV) Relative to Reactants ($H_2O^+ + NO_2$)

	PBE1PBE/ 6-311++g**	G3 (0 K)	QCISD(T)/ cc-pvtz	experimental
$NO_2^+(X^1\Sigma_g^+) + H_2O$	−2.59	−2.87	−3.11	−3.03
$NO_2^+(a^3B_2) + H_2O$	0.40	0.36		0.17
$NO_2H^+ + OH$	0.13	0.09	0.01	0.012
$NO^+ + HOOH$	−0.81	−1.47	−1.70	−1.67
$NO^+ + 2OH$	1.05	0.52	0.51	0.55
$NO^+ + O(^3P) + H_2O$	0.47	−0.01	0.65	−0.18
SC1	−3.44	−3.75	−3.97	
TC1	−1.40			
TS1	−1.11		−1.38	
TS2	−0.95			
TS3	−0.48			
TC2	−1.12			
TC3	−0.82			

termolecular reaction

$$NO_2^+ + H_2O + N_2 \rightarrow H_2NO_3^+ + N_2$$

$$k = 2\times10^{-27}\ \text{cm}^6\ \text{mol}^{-2}\ \text{s}^{-1}$$

This result implies that, not surprisingly, there is no barrier separating $NO_2^+ + H_2O$ (the CT products of the reaction here) from the complex labeled SC1 in Figure 1. Because of the high energy of TS1, it would not have been possible to produce the complex labeled $NO_3H_2^+$ under the thermal conditions of this study.

1. Singlet Reactions. The reaction expected to dominate in singlet collisions is CT, producing $NO_2^+ + H_2O$. Unlike atom-transfer reactions, where the collision geometry must allow bond formation, the highly exoergic CT reaction can occur in any orientation, and density of states considerations suggest that it should be highly efficient. The singlet complex labeled SC1, about 0.8 eV below the CT product energy, is essentially an electrostatically bound complex of the CT products, and statistical breakup of SC1 should go to CT products with essentially unit probability. The fact that the charge is localized on the NO_2 moiety in SC1 is obvious from the ONO bond angle (173°), which is much closer to that for NO_2^+ (180°) than that for NO_2 (134.1°). This raises the point that NO_2 bending is intimately coupled with any reaction coordinate that involves CT.

The covalently bound $NO_3H_2^+$ complex, connected to SC1 by a four-center TS1, might provide a route to other product channels on the singlet surface. Formation of $NO_3H_2^+$ by statistical isomerization from SC1 would be negligible because TS1 is both higher in energy and much tighter than the orbiting TS that controls separation to CT products. On the other hand, it is possible that $NO_3H_2^+$ might form directly in a small fraction of collisions that happens to occur with geometries allowing concerted N−O and O−H bond formation. If formed, this complex can decay via TS1 to CT products by OH elimination to NO_2H^+ or to $NO^+ + HOOH$ by a three-centered TS that we were unable to locate computationally. To obtain an estimate of the branching for decay of this complex and to obtain insight into the nature of the TS governing decay to $NO^+ + HOOH$, we calculated quasi-classical trajectories for unimolecular decay of highly excited $NO_3H_2^+$. A few 4000 step trajectories were examined for internal temperatures of 4000, 6000, 8000, 10000, 12000, and 14000 K, and on the basis of those results, a larger set of 35 trajectories was run at 8000 K, chosen as a reasonable compromise between dissociating within the 1.5 ps trajectory time and avoiding the sometimes bizarre initial conditions that result at higher temperatures. It should be noted that the average total internal energy in the complex at 8000 K corresponds to $E_{col} \approx 7$ eV, that is, about double the maximum studied experimentally. Of the 8000 K trajectories that dissociated to products during the integration period, the branching

dx.doi.org/10.1021/jp110523s |*J. Phys. Chem. A* 2011, 115, 1172–1185

between the three decomposition channels was (NO_2^+ + H_2O)/(NO^+ + HOOH)/(NO_2H^+ + OH) = 5:1:1, that is, decomposition is dominated by decay over TS1 to CT products. Because TS1 is a tight four-centered TS, the small branching to NO^+ + HOOH suggests that this TS (a tight three-center TS) must be rather high in energy, as indicated in Figure 1.

H^+ transfer should be possible by a direct scattering mechanism on either the singlet or triplet surfaces. H^+ transfer often proceeds near the collision rate in systems where it is exoergic.[29] Here, it is near-thermoneutral, the slight exoergicity being small compared to the available energy even at our lowest E_{col}. H^+ transfer products were a minor channel in the 8000 K $NO_3H_2^+$ trajectories; however, at the lower energies probed in the experiments, this high-energy decay channel would probably be negligible. Thus, we expect that any H^+ transfer that happens on the singlet surface will go by a direct mechanism, competing with the much more energetically favorable CT channel.

NO^+ can also form on the singlet surface. The NO^+ + HOOH channel probably requires mediation by the $NO_3H_2^+$ complex, but the trajectories together with inefficient formation of $NO_3H_2^+$, suggest that this mechanism should be minor. Note, however, that the NO_2H^+ product from H^+ transfer is only stable by ~0.48 eV with respect to OH elimination, producing NO^+ + 2OH with a net endoergicity of ~0.45 eV. To the extent that H^+ transfer occurs on the singlet surface, dissociation of the nascent NO_2H^+ product provides another singlet route to NO^+ production except at low E_{col}.

2. Triplet Reactions. On the triplet reaction coordinate, there is no facile exoergic process like CT competing with the atom transfer reactions; thus, atom transfer is expected to dominate the triplet reactions. There is a reactant-like triplet complex (TC1) where the charge is roughly equally distributed between the H_2O and NO_2 moieties. This complex can decay back to reactants or, via TS2 or TS3, toward products. TS2 and the resulting TC2 mediate proton transfer to the NO_2, generating NO_2H^+ + OH products. These H^+ products can presumably also form on the triplet surface by a direct mechanism. As discussed above, the nascent NO_2H^+ will dissociate to NO^+ + OH if its internal energy is greater than 0.48 eV.

There are several channels that involve CT or dissociative CT on the triplet surface. CT to produce $NO_2^+(a^3B_2)$ + H_2O is endoergic by 0.17 eV. This lowest-energy triplet state of NO_2^+ predissociates to NO^+ + O (^3P)[21] and would survive to be detected as NO_2^+ only if its internal energy were below ~80 meV. For higher $NO_2^+(a^3B_2)$ internal energies, the sequence of triplet CT followed by predissociation provides a route to NO^+ on the triplet surface, which we are calling sequential triplet dissociative CT. In addition to this endoergic sequential process, NO^+ can also be generated by a concerted triplet dissociative CT process. This reaction is concerted in the sense that the O-elimination step is concerted, going by TS3. The product of this transition is TC3, which is actually a bimolecular product consisting of an electrostatically bound $NO^+(H_2O)$ complex plus the free O (^3P) atom. This $NO^+(H_2O)$ complex dissociates to NO^+ + H_2O under beam conditions, but in the 300 K kinetics experiment, this complex is sometimes collisionally stabilized.

B. 300 K Kinetics. The 300 K rate constant is 1.3×10^{-9} cm^3 s^{-1} (unit reaction efficiency), in good agreement with past measurements;[10,11] however, we observe three reaction products, in contrast to the earlier work where only NO_2^+ was observed. NO_2^+ is the primary product, accounting for 70% (+8%/−11%) of the reaction. The remaining 30% is divided between two related products, NO^+, 20% (+7%/−4%), and $NO^+(H_2O)$, 10% (±4%). The asymmetric uncertainty limits reflect corrections for contributions from reactions of contaminant ions, discussed below.

The observation of both NO^+ and $NO^+(H_2O)$ clearly shows reaction on the triplet surface, and both are consistent with the concerted triplet dissociative CT channel shown in Figure 1. After passing over TS3, the stationary point labeled TC3 is $NO^+(H_2O)$ plus a free O (^3P) atom. If the nascent $NO^+(H_2O)$ has high internal energy and is not collisionally stabilized, then it dissociates to NO^+ + H_2O. Otherwise, it is detected as $NO^+(H_2O)$. The fact that the $NO^+(H_2O)/NO^+$ branching is 1:2 suggests that the nascent $NO^+(H_2O)$ is quite hot, such that it mostly dissociates before it can be stabilized by collisions with the He buffer gas (time between collisions ≈ 0.1 μs). This conclusion is consistent with the beam experiments, where no $NO^+(H_2O)$ is observed. We did not observe the H^+ transfer product NO_2H^+, even though this channel is slightly exoergic. It could be that this channel is suppressed by competition with the more energetically favorable NO^+ and $NO^+(H_2O)$ channels. We note, however, that NO_2H^+ is only bound by 0.48 eV with respect to NO^+ + OH, raising the possibility that it was destroyed by He buffer gas collisions in the flow tube. Dissociation is possible because there are enough collisions in the flow tube that dissociation processes requiring up to ~0.5 eV can be driven, albeit slowly, by the high-energy tail of the Boltzmann distribution.[30] Secondary CT of NO_2H^+ with NO_2 reactant may also convert some NO_2H^+ to NO_2^+ (see below). Experiments were done at low NO_2 pressures to minimize this secondary CT, but it cannot be entirely excluded.

Unlike the previous flow tube studies, we observe NO^+ and $NO^+(H_2O)$ products that clearly result from reactions on the triplet surface. Nonetheless, the 70% branching to NO_2^+ is still considerably larger than the 25% that would be expected from singlet CT, and the endoergicity of triplet CT (0.17 eV) is too large for it to make up the difference. Some of the "excess" NO_2^+ may result from secondary CT of NO_2H^+ products, but the high NO_2^+ yield suggests that a fraction of the triplet-coupled collisions (up to ~60% if secondary CT of NO_2H^+ is neglected) may undergo transition to the singlet surface during thermal energy collisions, leading to CT products. Efficient triplet → singlet conversion in a system with weak spin−orbit coupling might be possible if the triplet reaction coordinate (Figure 1) results in mediation by long-lived complexes. TC1 and TC2 presumably interconvert rapidly via TS2 under thermal conditions; thus, the rate-limiting TS must be TS3. We estimated the lifetime of complex TC1 with respect to decay over TS3 using an RRKM calculation[31] based on the theoretical energies and vibrational frequencies for TC1 and TS3. For E_{col} ≈ 0 and an angular momentum corresponding to thermal energy capture collisions, the RRKM lifetime is ~110 ps. As shown below, the beam experiments can be explained without invoking triplet → singlet conversion, reflecting the fact that the minimum E_{col} in the beam work is an order of magnitude higher, which increases the rate of passage over TS3 by an order of magnitude. Furthermore, two additional triplet product channels are open even at the lowest E_{col} probed in the beam experiments, decreasing the TC1 lifetime into the <5 ps range. Assuming that the triplet → singlet conversion rate is independent of E_{col}, the shorter collision time would result in <~4% of triplet collisions converting to the singlet surface.

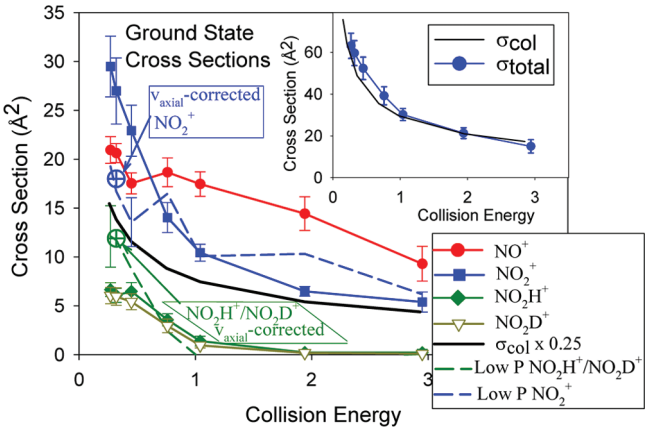

Figure 2. Integral cross sections for production of NO_2^+, NO^+, NO_2H^+, and NO_2D^+ in reaction of ground-state H_2O^+ with NO_2. The dashed lines are low-pressure measurements, and the circled crossed data points (blue and green for CT and DT, respectively) are integral cross sections extracted from simulation of vaxial distributions (Figures 3−5), accounting for survival. The inset compares the total reaction cross section (σ_{total}) with the collision cross section (σ_{col}).

In the previous flow tube experiments, contaminant primary ions almost certainly played a role. In the Dotan et al. paper,[10] the H_2O^+ was made in the flow tube by CT between He^+ and water, and the paper notes that "H_2O^+ ions were among the abundant species". He^+ CT with water produces ∼83% OH^+, which therefore must have been a major reactant ion in this FDT experiment. Because it is known that OH^+ produces both NO^+ and NO_2^+,[11] it is probable that the reactions leading to NO^+ and NO_2^+ were not correctly identified. While the Shul et al.[11] work was done in a SIFT, they state that it was not possible to separate OH^+, H_2O^+, and H_3O^+ in the reactant ion selection quadruple; thus again, all three ions were present in the flow tube simultaneously.

C. Integral Cross Sections and Product Branching. The integral cross sections for production of NO^+, NO_2^+, NO_2H^+, and NO_2D^+ in reaction of ground-state HOD^+ with NO_2 are shown in Figure 2 over the center-of-mass collision energy range from 0.27 to 2.94 eV. The inset of the figure compares the total reaction cross section (σ_{total}) with the collision cross section (σ_{col}), which is calculated as the capture cross section ($\sigma_{capture}$), including ion-induced dipole and rotationally averaged ion−dipole forces, using the method of Troe.[32] The hard-sphere cross section (calculated from orientation-averaged contact distances for HOD^+ and NO_2, assuming covalent radii) is not shown because it exceeds $\sigma_{capture}$ only for E_{col} > 3.4 eV. Note that σ_{total} is essentially equal to σ_{col}, indicating that both singlet and triplet reactions proceed at near-unit efficiency. For comparison, the mainframe of the figure also shows the singlet collision cross section, that is, 25% of σ_{col}.

While both the thermal kinetics and beam experiments indicate essentially unit reaction efficiency, the product branching is quite different. In the beam experiment, NO^+, primarily resulting from triplet reactions, is the dominant channel over most of the energy range, out-competed by NO_2^+ only at low E_{col}. The NO_2H^+ and NO_2D^+ channels have similar magnitudes and together amount to ∼20% of the σ_{total} at low E_{col} but drop to negligible values above 1 eV. Despite being less exoergic, H^+ transfer is slightly more efficient than D^+ transfer. If the mechanism were complex-mediated, the branching might reflect the ∼10% higher density of states for the H^+ transfer products. In a direct mechanism, the collision dynamics might favor $NO_2H^+ + OD$.

The difference in branching between the SIFT and beam experiments is attributable to two factors. The much longer collision times at thermal energies increases the likelihood of triplet → singlet conversion, which results mostly in production of NO_2^+. Furthermore, there are several moderately endoergic channels that are reasonably efficient at the energies probed in the beam study but which are either energetically inaccessible or depleted by competition in the thermal measurements. When these factors are considered, the two data sets are consistent with each other and also with the reaction coordinate in Figure 1.

One obvious point is that, in the beam experiments, the cross sections for NO_2^+ and NO^+ are both significantly larger than $0.25\sigma_{col}$, implying that both these reactions have significant contributions from collisions on the triplet surface. For NO^+, this is no surprise because most of the processes that could potentially contribute are on the triplet surface (concerted and sequential dissociative CT, secondary dissociation of NO_2H^+). The magnitude of the NO_2^+ cross section is more surprising, however, because we expect that the dominant contribution to NO_2^+ should be singlet CT. Under beam conditions, endoergic triplet CT is also possible; however, the NO_2^+ (a^3B_2) product would predissociate[21] and be detected as $NO^+ + O$ (^3P) unless it were produced with internal energy below ∼80 meV. Such collisions are certainly possible, particularly at low E_{col}, but it seems unlikely that triplet CT could account for such a large contribution to NO_2^+.

Instead, we attribute most of the "excess" NO_2^+ to a secondary CT reaction. Our normal scattering cell pressure (0.1 mTorr) is as low as practical, given the low mode-selected primary ion intensities. The probability that reactant ions make a single collision with NO_2 at this pressure is ∼3.5%, but for product ions that are generated with near-zero lab velocity, there is a high probability of being hit by thermal NO_2 as they slowly exit the scattering cell. In this case, the slow products can react

$$NO_2H^+ + NO_2 \rightarrow NO_2^+ \rightarrow NO_2H \qquad \Delta H = -1.28 \text{ eV}.$$

We tested the effect of this reaction on the NO_2H^+, NO_2D^+, and NO_2^+ channels by measuring the cross sections for reaction of ground-state HOD^+ at a scattering cell pressure 1 order of magnitude lower than normal, and the resulting cross sections are indicated by dashed curves in Figure 2. One curve shows the low-pressure cross sections for both NO_2H^+ and NO_2D^+ (which were identical within the rather large uncertainty), and the other shows the low-pressure NO_2^+ cross section. The NO_2H^+ and NO_2D^+ cross sections increase at low pressure, consistent with lower probability of being converted to NO_2^+ by secondary CT, and there is a concomitant decrease in the NO_2^+ cross section. Additional insight into the effect of this secondary reaction is obtained from the recoil velocity data.

D. Recoil Velocity Distributions and Reaction Mechanisms. Considerable insight into the reaction mechanisms is provided by measurements of the product ion recoil dynamics, which also allow a more quantitative analysis of issues such as secondary reactions. Figures 3−6 give the laboratory frame axial projections of the recoil velocity distributions for the NO_2D^+, NO_2H^+, NO_2^+, and NO^+ product ions measured at select collision

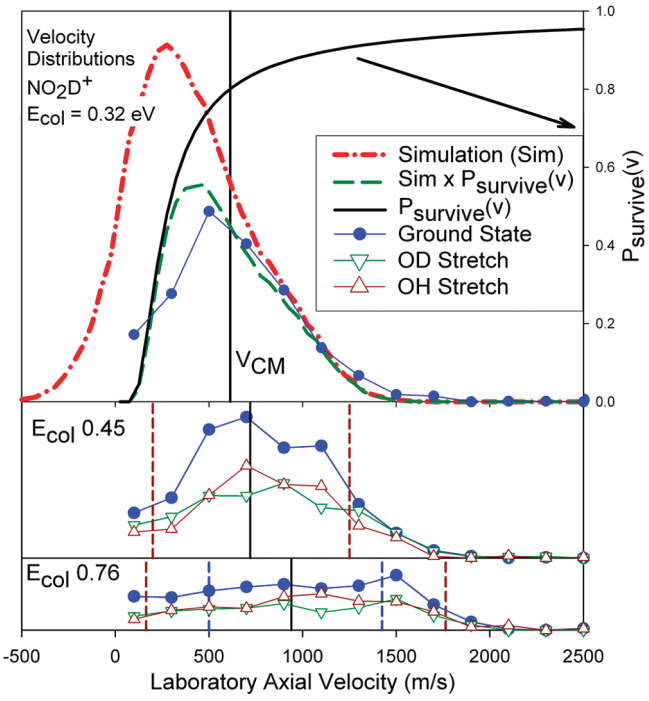

Figure 3. Lab frame v_{axial} distributions for the NO_2D^+ product, scaled to be proportional to the integral cross section for each energy and vibrational state. Points are experimental; the smooth red dash−dot curve is from simulations, and the green dashed line is the simulation multiplied by the survival probability ($P_{survive}$). The heavy vertical line in each frame indicates the lab velocity of the center-of-mass frame ($\langle V_{cm} \rangle$), and the dashed vertical lines give the recoil velocity limits for NO_2D^+ dissociation for ground-state and OH-stretch-excited HOD^+.

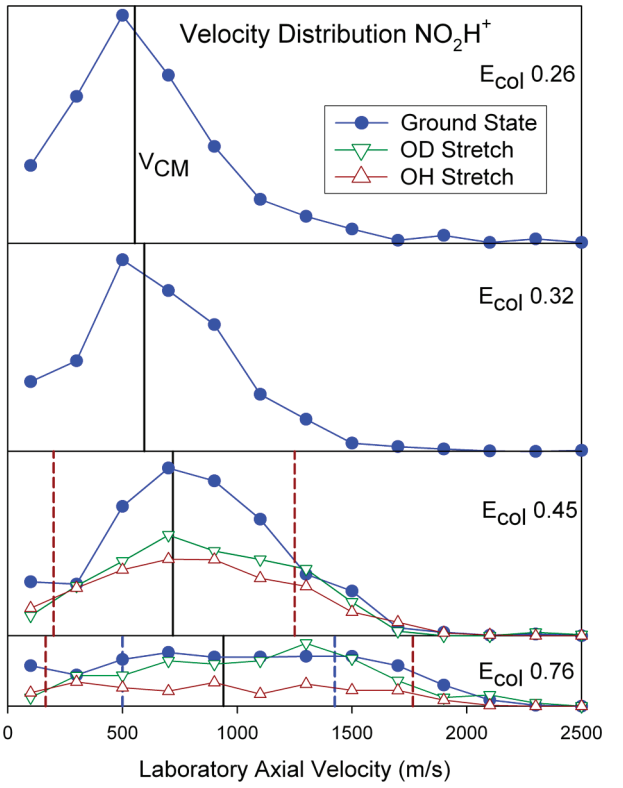

Figure 4. Lab frame v_{axial} distributions for the NO_2H^+ product, scaled to be proportional to the integral cross section for each energy and vibrational state. The heavy vertical line in each frame indicates the lab velocity of the center-of-mass frame ($\langle V_{cm} \rangle$), and the dashed vertical lines give the recoil velocity limits for NO_2H^+ dissociation for ground-state and OH-stretch-excited HOD^+.

energies. The data series with points are experimental, and the smooth curves shown in some frames are simulations, discussed below. The black vertical line in each frame indicates the laboratory frame velocity of the center-of-mass ($\langle V_{cm} \rangle$), averaged over the collision energy distribution. Axial velocity (v_{axial}) distributions are simply the projections of the full velocity distributions on the ion guide axis. Because the experiment has axial symmetry, the raw distributions directly reveal the qualitative dynamics. For example, ions that are faster (slower) than V_{cm} correspond to forward (backward) scattering of the product ion with respect to the reactant ion beam direction. Because we measure the scattering of the product ions, if the charge transfers in the reaction (i.e., for all product channels here), the definitions of forward and backward are opposite of the usual convention. For example, H^+, D^+, or electron transfer occurring in large-impact-parameter collisions, where momentum transfer is necessarily small, will result in product ions with near-zero lab velocities, corresponding to backward scattering in the center-of-mass frame. Conversely, rebounding dynamics, as might occur in small-impact-parameter collisions, will produce fast, forward-scattered product ions. Reactions mediated by a long-lived complex must result in v_{axial} distributions that are forward−backward symmetric about V_{cm}.

Ions that are backscattered in the lab frame are reflected by the injection electrode at the entrance of the ion guide and detected at long times, corresponding to apparently low velocities. The low-velocity region (below ~500 m/s) also has the worst perturbations from stray fields and, as discussed above, is most likely to be affected by secondary collisions. For these reasons, the portion of the velocity distribution below ~500 m/s must be interpreted with these factors in mind. Because this system has a light projectile and heavy target, V_{cm} is at low lab velocity, particularly at low E_{col}, with the result that a substantial fraction of the product ions appears below 500 m/s.

1. H^+/D^+ Transfer Reaction. NO_2H^+ and NO_2D^+ together account for about 20% of σ_{total} at low energies (38% in the low-pressure measurement), falling to <3% at the highest energies. This channel produces two doublet species; therefore, it correlates to both the triplet and singlet surfaces. The singlet reaction could go by a direct mechanism or could involve formation of the $NO_3H_2^+$ complex, followed by OH (OD) elimination. As argued above, the $NO_3H_2^+$ complex probably does not form very efficiently, and once formed, trajectory analysis suggests that it would decompose mostly back to SC1 and CT products. The available energy is much lower as the system traverses the triplet reaction coordinate; thus, for low E_{col}, the triplet complexes TC1 and TC2 have significant lifetimes (~5 ps at our lowest E_{col}). H^+/D^+ transfer can probably also occur in direct triplet collisions, without significant mediation by the complexes.

Direct and complex-mediated H^+/D^+ transfer should result in very different v_{axial} distributions. Direct H^+ or D^+ transfer might be expected to give NO_2H^+ or NO_2D^+ that is strongly backscattered in the CM frame because the light H^+ or D^+ carries little momentum. (As noted, because the charge transferss in this reaction, small-angle scattering corresponds to backward scattered ions). In the limit of spectator stripping,[33] the product ions would appear near zero lab velocity. In contrast, H^+/D^+

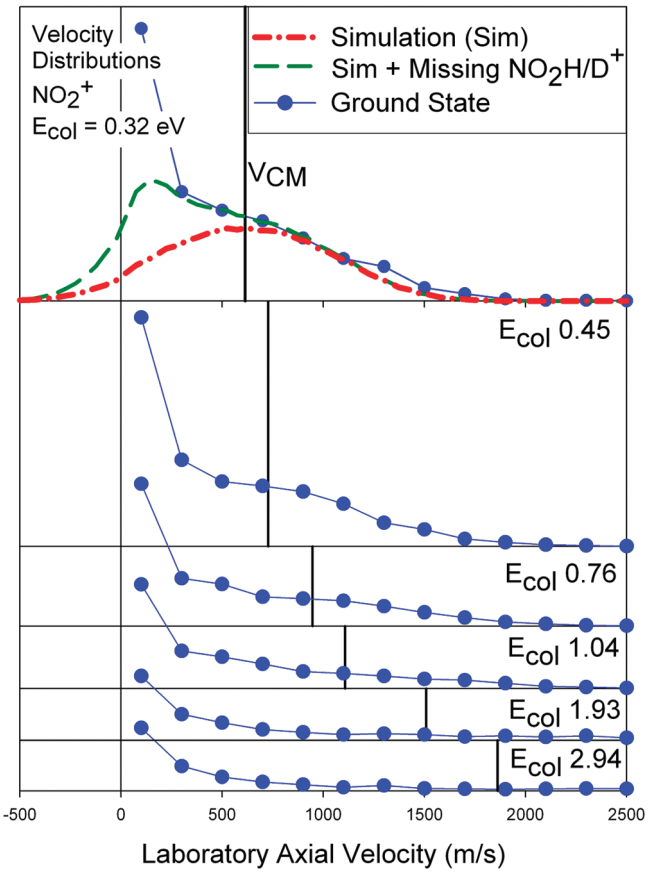

Figure 5. Lab frame v_{axial} distributions for the NO_2^+ product, scaled to be proportional to the integral cross section for each energy and vibrational state. Points are experimental; the smooth red dash−dot curve is from simulations, and the green dashed line is the simulation plus the fraction of the NO_2D^+ and NO_2H^+ products that is converted to NO_2^+ by secondary reactions. The heavy vertical line in each frame indicates the lab velocity of the center-of-mass frame ($\langle V_{cm} \rangle$).

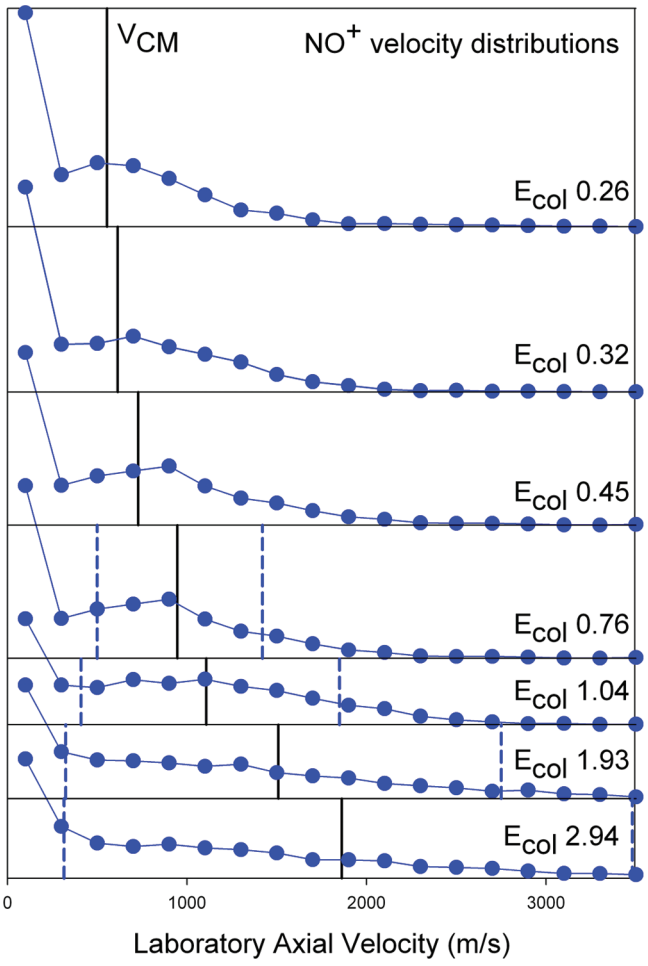

Figure 6. Lab frame v_{axial} distributions for the NO^+ product, scaled to be proportional to the integral cross section for each energy and vibrational state. The heavy vertical line in each frame indicates the lab velocity of the center-of-mass frame ($\langle V_{cm} \rangle$), and the dashed vertical lines give the recoil velocity limits for NO_2H^+ dissociation for ground-state HOD^+.

transfer mediated by a long-lived complex must generate products that are forward−backward-symmetric with respect to V_{cm}.

The v_{axial} distributions for the $NO_2D^+ + OH$ channel are shown in Figure 3, and the analogous distributions for the $NO_2H^+ + OD$ channel are in Figure 4. Distributions at higher E_{col} are not plotted because the cross sections for these channels are too low to give useful distributions. Consider the top frame of Figure 3, which gives the v_{axial} distribution for reaction of ground-state HOD^+ at E_{col} = 0.32 eV. The experimental distribution looks reasonably forward−backward-symmetric, which would tend to suggest that complex-mediated D^+ transfer is dominant. The rough forward−backward symmetry also appears at higher E_{col} and for the NO_2H^+ distributions in Figure 4. It is important, however, to consider the effects of secondary reactions, which were shown (Figure 2) to be reacting away almost half of the nascent NO_2D^+ and NO_2H^+ products formed at low E_{col}.

a. Secondary Reactions. The probability that a NO_2H^+ or NO_2D^+ product ion will survive passage out of the scattering cell is highly dependent on its velocity because decreasing velocity increases the capture cross section and also increases the residence time in the cell. The effects of thermal target motion on collision probability in a beam gas configuration were summarized by Ramsey, and we follow the development given there.[34] The probability of passing *without* collision through a gas cloud of length l at velocity v is

$$P_{survive}(v) = e^{-l/\lambda_v}$$

where λ_v is the mean free path, including the effects of thermal target motion

$$\lambda_v = \pi^{1/2} \frac{(v/\alpha_G)^2}{n_G \sigma_{BG} \psi(v/\alpha_G)}$$

where α_G is the average thermal speed of the neutral target molecules, n_G is the number density of the neutral target, σ_{BG} is the collision cross section, and $\psi(v/\alpha_G)$ is

$$\psi(x) = x e^{-x^2} + (2x^2+1) \int_0^x e^{-y^2}\, dy$$

Here, σ_{BG} is assumed to be the velocity-dependent capture cross section, and l is the distance from the center of the scattering cell to its end, which is a lower limit on the average distance that

a scattered ion might have to travel to exit the gas cloud. Large lab scattering angles will, of course, increase the path length and therefore decrease the survival probability.

The top frame of Figure 3 shows the results. The black curve, plotted against the right-hand axis, shows the probability that NO_2D^+ survives without conversion to NO_2^+, assuming the limit that every capture collision leads to reaction. Note that for lab velocities greater than ~500 m/s, the secondary collision probability is low, and therefore, the survival probability is high. At lower velocities, $P_{survive}$ drops rapidly to zero, indicating that the portion of the v_{axial} distribution that is backward-scattered with respect to V_{cm} should be significantly attenuated by conversion to NO_2^+. We can use $P_{survive}$ to reconstruct what the v_{axial} distribution would look like if there were no secondary collisions. The green dashed curve, which is a reasonable fit to the experimental data, was obtained by multiplying the red dashed curve by $P_{survive}$, that is, the "true" v_{axial} distribution must look something like the red dashed curve. This red curve was generated from a dynamical model and was convoluted with the velocity distributions of the ion beam and target gas to allow direct comparison with experiment.[35,36]

The dynamical model used assumed a stripping-like process, wherein NO_2D^+ recoils with a velocity distribution peaking at 180° with an angular distribution symmetric about 180° with a half width of 40°. The recoil energy distribution was assumed to be a Gaussian peaking at 70% · E_{avail} with a width of ~20% · E_{avail}, where E_{avail} is the total energy available in the product channel. For comparison, the spectator stripping limit would give products at 180° with a velocity corresponding to 77% of E_{avail} in recoil (83% for NO_2H^+). In contrast, reaction mediated by a long-lived complex would give an isotropic angular distribution and would tend to partition a statistical fraction (~13%) of E_{avail} into recoil.

We certainly do not claim to be able to quantitatively extract the "true" v_{axial} distributions by this process; however, two points are clear. The true distributions are significantly backward-peaked, implying domination by a direct stripping-like D^+ transfer mechanism. There may also be a small component of complex-mediated D^+ transfer producing products near V_{cm}, but this cannot account for more than ~30% of the total reaction, even for this low E_{col}.

As a check on the model, it is useful to estimate the increase in the D^+ transfer integral cross section that would result if there were no secondary reactions. This increase is simply the ratio of the area under the red and green dashed curves, and this "corrected" value of the integral cross section has been plotted as a single data point in Figure 2, which is in gratifyingly good agreement with the cross section curve extracted from the low-pressure measurements (dashed dark green curve, Figure 2).

In principle, such corrections could be made for all of the v_{axial} distributions; however, given the ambiguity inherent in guessing the correct form of the model distributions, we do not feel that this level of interpretation is warranted. It is clear, however, that all of the v_{axial} distributions for both NO_2D^+ and NO_2H^+ must be significantly backward-peaked and, therefore, that D^+ or H^+ transfer goes predominantly by a direct mechanism at all energies where these channels are significant.

b. Sequential Dissociation. Another interesting feature of the NO_2H^+ and NO_2D^+ channels is that their cross sections drop rapidly with increasing energy, to essentially zero by 2 eV. More typically, proton-transfer cross sections tend to have E_{col} dependence that tracks that of σ_{col},[37−40] unless some other process is in competition. In this case, the competing process is secondary decomposition of the nascent NO_2H^+ and NO_2D^+ product ions, if they are produced with too much internal energy

$$NO_2D^+ \rightarrow NO^+ + OD \qquad \Delta H_{rxn}(0K) = +0.53 \text{ eV}$$

$$NO_2H^+ \rightarrow NO^+ + OH \qquad \Delta H_{rxn}(0K) = +0.48 \text{ eV}$$

The fact that the NO_2H^+ and NO_2D^+ signals essentially disappear as E_{col} is raised between 1 and 2 eV is consistent with the model recoil dynamics used to fit the v_{axial} distribution at low E_{col} in Figure 3, where we assumed that an average of ~70% of E_{avail} is partitioned to recoil energy, leaving ~30% in internal energy. Given the high frequency of the OH or OD stretches, it is expected that most of this internal energy should go into the NO_2D^+ or NO_2H^+ products, and in that case, it is not surprising that these products have largely disappeared by $E_{col} \approx 1$ eV. The effect of this dissociation can also be seen directly in the v_{axial} distributions in Figures 3 and 4. For $E_{col} \leq 0.5$ eV, the available energy is too low for there to be any dissociation of the NO_2H^+ or NO_2D^+ product ions, at least for the ground-state reaction. At higher E_{col}, however, those product ions with low center-of-mass recoil velocities, and therefore high internal energies, should start to dissociate. This effect is clearly seen in the v_{axial} distributions for NO_2H^+ and NO_2D^+ at E_{col} = 0.76 eV. The dashed vertical blue lines near 425 and 1475 m/s lab velocity indicate the limits of this process for the ground-state reaction; ions with higher center-of-mass recoil velocities (i.e., outside of the two lines) cannot decompose, while those inside will decompose if most or all of the internal energy is partitioned to the NO_2H^+ or NO_2D^+ product. The odd, flat-topped v_{axial} distributions reflect the fact that much of the NO_2D^+ or NO_2H^+ within the limit lines is missing due to dissociation. The issue of energy partitioning in the products as probed by this dissociation process is discussed in more detail in the section on vibrational effects.

2. Charge Transfer. Singlet CT is quite exoergic in this system, and triplet CT is only slightly endoergic. For exoergic CT, a long-range electron hopping mechanism is sometimes active, and one signature of this mechanism is product ions created at near-zero laboratory velocities because the electron carries little momentum. When long-range transfer is efficient, the CT cross section can significantly exceed the hard-sphere or capture collision cross sections.[38] Figure 5 shows the v_{axial} distributions for the NO_2^+ signal for select E_{col} values. Note the apparent peak at velocities near zero, which ordinarily might be evidence of a long-range mechanism. In this case, however, we know that secondary reactions convert slow NO_2H^+ and NO_2D^+ to NO_2^+, which is also expected to be slow. As a result, some fraction of the near-zero v_{axial} peak is certainly due to this artifact. The contribution of the secondary reaction can easily be tested using the same approach used above to simulate its effect on the NO_2D^+ v_{axial} distribution, and the result is shown in the top frame of the figure. The red curve is a model of the "true" v_{axial} distribution, based on assuming isotropic scattering and adjusting the distribution of recoil velocities to fit the forward-scattered half of the distribution, which is essentially unaffected by the secondary reaction artifact. We then added the contribution from NO_2D^+ and NO_2H^+ products that underwent secondary reaction to generate NO_2^+ (i.e., twice the difference between the red and green curves in Figure 3). For this purpose, we also assumed that the resulting NO_2^+ velocity was, on average, identical to that of the NO_2D^+ or NO_2H^+ from which it came. The result is the

green curve that fits the experimental data down to ~200 m/s. Note that the simulation predicts significant intensity of products that are scattered to negative lab velocities, which appear at small but positive velocities in the experiment. If this negative component of the simulation is assumed to contribute to the near-zero peak in the experiment, then the simulation fits the experimental data reasonably well. Furthermore, if we use this process to estimate the value of the "true" integral cross section, the result is in excellent agreement with the experiments done at low pressures (see single data point in Figure 2).

The nature of the model used for the "true" distribution in this simulation suggests that CT occurs predominantly in intimate collisions. Because the SC1 complex is weakly bound with respect to products, it is doubtful that it could have a long enough lifetime (>~1 ps) to account for a forward−backward-symmetric NO_2^+ v_{axial} distribution. Note, however, that while complex mediation must result in forward−backward symmetry, the converse is not true (cf. hard-sphere scattering). We suggest that CT probably goes by a direct mechanism involving intimate collisions over a range of impact parameters, resulting in a recoil velocity distribution that just happens to look forward−backward-symmetric in a measurement of only the axial component, as in our experiment.

The absence of long-range CT in this system is not surprising. Long-range CT is essentially an electronic transition where the initial and final orbitals happen to be on different centers; thus, one requirement is reasonable Franck−Condon (FC) factors connecting the initial state with near-resonant final states. The requirement for near-resonant final states is because there cannot be significant translational ↔ internal energy transfer at long-range because the intermolecular forces are too weak. In this system, the HOD bond angle changes by <4°, and the OH/OD bond lengths change by only ~0.03 Å in going from H_2O^+ to H_2O; thus, its part of the FC distribution is dominated by the diagonal (vibrational-state-preserving) transition.[41] In contrast, the ONO bond angle changes from 134.1° in NO_2 to linear in NO_2^+, and the NO bond lengths also decrease by 0.075 Å. For this reason, the NO_2 bend is FC-active, as is the symmetric stretch to a lesser extent. Judging from the photoelectron spectrum,[42] the states with good FC factors in the NO_2 → NO_2^+ transition lie in the range between ~1 and ~2.4 eV above the ground state. The CT exoergicity in this system is 3.03 eV, and as a result, there is poor FC overlap between $HOD^+ + NO_2$ and the near-resonant $HOD + NO_2^+$ states, thus rendering the long-range mechanism inefficient.

As E_{col} is increased, the CT v_{axial} distributions shift gradually into the backward hemisphere. This trend is obvious at 1.93 eV, where rapid dissociation of the NO_2H^+ and NO_2D^+ products means that their contribution to the NO_2^+ signal can be neglected. Here, the NO_2^+ peaks near zero lab velocity, but in a very broad distribution extending well forward of V_{cm}. This pattern suggests that CT occurs at the full range of impact parameters ranging from head-on (giving $v_{axial} > V_{cm}$) to grazing (v_{axial} near zero). The fact that the grazing collisions dominate simply reflects the fact that the probability for colliding at impact parameter b is proprortional to b.

Note that at 2.94 eV (bottom frame of Figure 5), the distribution is narrower (more backward peaked) than that at lower energies, even though the energy available to drive recoil is higher. This disappearance of NO_2^+ with v_{axial} near V_{cm} almost certainly indicates the onset of singlet dissociative CT ($NO^+ + O(^1D) + H_2O$), which becomes possible for $E_{col} > 1.78$ eV. This process can only occur for collisions where most of the available energy is partitioned to the internal energy of the nascent NO_2^+, that is, collisions producing NO_2^+ with v_{axial} near V_{cm}.

The remaining question is to what extent the exoergic singlet and endoergic triplet channels contribute to the total CT cross section. From the fact that the NO_2^+ cross section is larger than the singlet collision cross section (Figure 2), even after correction for secondary reaction of NO_2H^+ and NO_2D^+, it is clear that there must be some contribution from triplet CT. At low collision energies, we might expect that triplet CT should be a minor channel on the triplet surface because it is competing with three lower-energy channels (dissociative CT, H^+ and D^+ transfer, and dissociation back to reactants). Because $\sigma_{total} \approx \sigma_{col}$ (Figure 2, inset), dissociation back to reactants can be neglected, but the other competing channels have low-energy transition states and are major channels at low E_{col}. At high E_{col}, triplet CT probably is a reasonably efficient process. As noted above, however, the NO_2^+ (a^3B_2) product ion would predissociate to be detected as NO^+ ($+O(^3P)$), unless produced with vibrational excitation < ~80 meV.[21] Because relatively hard collisions are required to drive endoergic triplet CT, it seems likely that most of the triplet NO_2^+ produced at high E_{col} would dissociate and contribute to the NO^+ signal.

In summary, the NO_2^+ production cross section, corrected for the $NO_2H^+/NO_2D^+ \rightarrow NO_2^+$ secondary reaction, is only ~20% greater than the singlet collision cross section. On the singlet surface, CT is likely to be highly efficient because it is a facile process that can occur in any collision geometry, and the competing atom-transfer channels are either much higher in energy (H^+/D^+ transfer) or likely to occur only in very restricted collision geometries ($NO^+ + HOOH$). Therefore, the amount of "excess" NO_2^+ that cannot be attributed to singlet reactions is small and likely to be accounted for by the fraction of triplet CT products that are produced with low levels of vibrational excitation. There is no compelling need to invoke triplet → singlet transitions during the collisions, presumably because the collision times are much shorter than those in the 300 K kinetics experiments.

3. NO^+ Production. There are five processes that appear to contribute to the NO^+ signal in different energy ranges. Because the NO^+ cross section is roughly double the singlet collision cross section, it is clear that at least half of the NO^+ signal must result from triplet reactions. One process that can only occur on the singlet surface is O^- abstraction, producing $NO^+ + HOOH$. One pathway to this product channel would be formation of the $NO_3H_2^+$ complex, followed by HOOH elimination, and this channel is seen in trajectories starting with highly excited $NO_3H_2^+$. This complex is not likely to form in a statistical mechanism because it is in competition with a much lower energy and a more facile process, dissociation to CT products. This channel is not likely to be efficient in direct collisions either because it is likely to occur only in a narrow range of collision geometries, whereas CT has no geometry requirements. To the extent that it does occur, the complex-mediated route would give NO^+ near V_{cm}, and the direct route probably would give NO^+ in a broader distribution about V_{cm} because intimate collisions would be required.

Another minor singlet route to NO^+ is dissociative CT to $NO^+ + O(^1D) + H_2O$, which does appear to occur at high E_{col}, as discussed above. On the other hand, because the CT cross section shows no sign of a significant drop above the threshold for this process (1.78 eV), we conclude that it is too inefficient to

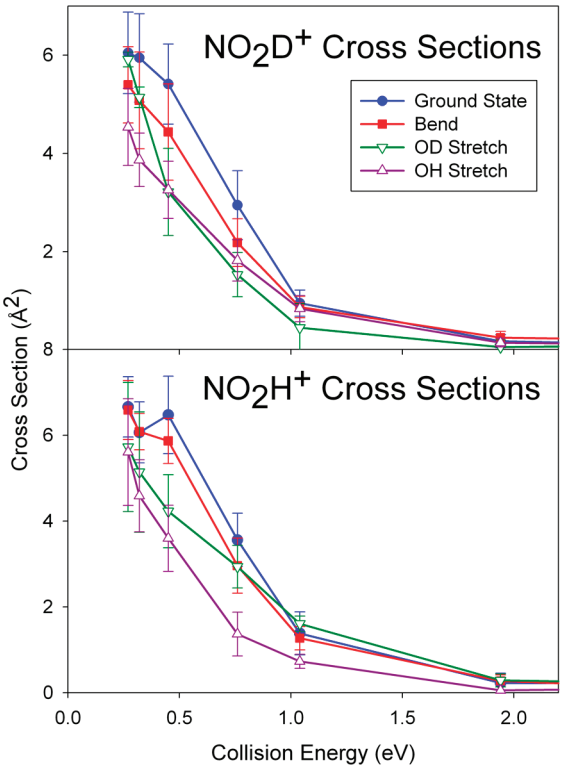

Figure 7. Effects of different HOD^+ vibrational levels on the cross sections for NO_2D^+ (top frame) and NO_2H^+ (bottom frame).

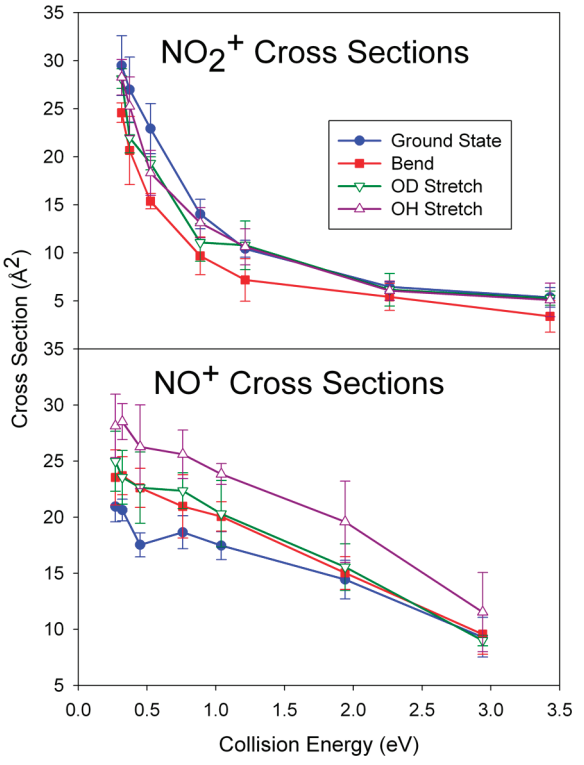

Figure 8. Effects of different HOD^+ vibrational levels on the cross sections for NO_2^+ (top frame) and NO^+ (bottom frame).

make a significant contribution to the NO^+ channel. It would produce NO^+ with recoil velocities near V_{cm}.

The final possible singlet (or triplet) reaction would be H^+ or D^+ transfer, followed by OH or OD elimination from the NO_2H^+ or NO_2D^+ product. This process clearly happens, as discussed above, however, because singlet CT is much more energetically favorable than singlet H^+ or D^+ transfer; we expect that most NO_2H^+ or NO_2D^+ production occurs by triplet reactions. In either case, NO^+ cannot form this way at E_{col} < ~0.55 eV, but at higher energies, there should be NO^+ with v_{axial} in a broad distribution around V_{cm} because parent NO_2H^+ or NO_2D^+ must have high internal energy, corresponding to low recoil velocity.

On the triplet surface, there are two other reactions that we believe to be responsible for most of the NO^+. A major triplet channel, and the most exoergic, is concerted dissociative CT, mediated by TC1 and controlled by TS3, and, as shown by the flow tube results, it definitely involves the product-like complex TC3, at least for low collision energies. This process should contribute NO^+ with forward−backward-symmetric v_{axial}; however, it is probable that the mechanism becomes direct at high energies, and in that case, it is likely that the product ion is backscattered (slow in the lab) because it should be possible in grazing collisions. The sequential triplet dissociative CT mechanism should also be significant, particularly at higher energies. We expect the nascent NO_2^+ (a^3B_2) to be backscattered in the center-of-mass frame (low lab velocity); thus, the resulting NO^+ should also be slow in the lab frame.

On the basis of these dynamical considerations, it is possible to at least partly unravel the contributions from the five possible channels to the NO^+ v_{axial} distributions shown for reaction of ground-state HOD^+ in Figure 6. At collision energies up to ~0.5 eV, where only concerted triplet dissociative CT and singlet HOOH elimination are likely to be significant, the distributions show a broad, forward−backward-symmetric component. The spike at low lab velocity can be attributed, at least in part, to ions in the main velocity component that scattered at negative lab velocities and were detected after reflection at the ion guide entrance. For reasons discussed above, we believe that singlet NO^+ + HOOH production is probably not particularly efficient, and therefore, the large NO^+ signal at low E_{col} is mostly attributed to concerted triplet dissociative CT. This channel should produce NO^+ in a forward−backward-symmetric velocity distribution, as observed. With increasing E_{col}, the v_{axial} distributions become backward-peaked, although at all energies, there is substantial intensity in a broad component near, but not symmetric about, V_{cm}. The broad component near V_{cm} is attributed to NO^+ from decomposition of nascent NO_2H^+ and NO_2D^+ products, with a small contribution from singlet dissociative CT. The backscattered NO^+ peak at low lab velocities is attributed to the combined contributions from concerted and sequential triplet dissociative CT.

E. Vibrational Effects. Figures 7 and 8 show the cross sections for the individual channels in reaction of HOD^+ in its 000, 001, 010, and 100 vibrational states. The 001 level has mostly OH stretch character and is the highest-energy mode at 397 meV. The 010 level is the bend at 153 meV, and the 100 level has mostly OD stretch character at 293 meV. The effects of vibration are mode-specific, quite distinct from the effects of collision energy, and qualitatively different for the different product channels. The NO^+ channel is enhanced by all three modes of excitation, with the largest enhancement from the OH stretch and intermediate but similar effects from the OD and bend excitations, despite the factor of ~2 difference in energy.

The CT channel is inhibited by all modes, with the largest effect from the lowest-energy bend mode. The NO_2H^+ and NO_2D^+ channels are also inhibited by all modes, but the OH and OD stretch modes have different effects for the two channels, giving insight into how reactant vibration couples to product internal energy, as outlined below.

Within experimental error, there is no vibrational effect on σ_{total} at low energies, which is not surprising because $\sigma_{total} \approx \sigma_{col}$. Therefore, the vibrational effects reflect changes in the competition between the various product channels. Above 1 eV, the other modes continue to have negligible effects on total reactivity; however, excitation of the OH stretch results in a ~10% increase in total cross section.

One might expect that the branching between NO_2D^+ and NO_2H^+ should be mode-dependent and particularly that excitation of the OH stretch would enhance NO_2H^+, while OD stretch excitation would enhance NO_2D^+. As discussed in the Introduction, such effects were seen for HOD with both overtone and fundamental excitations. In those systems, there are significant barriers to H/D transfer associated with the need to partially break the OH or OD bond before significant energy is recovered by making the new HH or HCl bonds. Therefore, stretching an OH or OD bond effectively reduces the barrier height for transfer of H or D, respectively. In contrast, H^+/D^+ transfer in this system is essentially thermoneutral and, more importantly, is a barrierless process. The competition between H^+ and D^+ transfer and of those channels with CT and so forth probably depends to a large extent on the orientation during collision and whether the reactants come together in singlet or triplet coupling. If the orientation is optimal for H^+ transfer (i.e., ONO−H−OD), then H^+ transfers, collision in ONO−D−OH geometries leads D^+ transfer, and orientations where neither H nor D impact an O atom in NO_2 presumably lead to CT or NO^+ products.

As discussed above, the strong suppressing effect of E_{col} on the NO_2H^+/NO_2D^+ channels results from dissociation of the nascent product ion, if its internal energy is greater than the energy required to eliminate OH/OD (~0.53 eV/0.58 eV). HOD^+ vibrational excitation also suppresses the NO_2H^+/NO_2D^+ channels (Figures 7 and 8), presumably for the same reason, and the mode dependence of this suppression provides insight into how different HOD^+ modes couple to the internal energy of the two product moieties. We first consider how vibrational excitation affects the v_{axial} distributions, as shown in the lower frames of Figures 3 and 4. Results are shown only for the OH and OD stretch modes, both because they have the largest effects on the cross sections and because they have different effects on the two channels.

Consider the data for NO_2D^+ in the bottom two frames of Figure 3. At E_{col} = 0.45 eV, we would expect reaction of ground-state HOD^+ to result in a negligible fraction of NO_2D^+ with enough energy to dissociate; however, addition of one quantum of either the OH (397 meV) or OD (293 meV) stretch opens this dissociation channel, but only for those collisions where most of E_{avail} is partitioned to internal energy. These correspond to collisions with v_{axial} near V_{cm}, and the two vertical lines symmetrically displaced from V_{cm} enclose the region where dissociation is possible for OH excitation. Clearly, over this region of the recoil velocity distribution, the intensities from OH or OD excited reactions are significantly reduced. It is interesting to note that the attenuation from OD stretch excitation is actually larger than that from the OH stretch, even though the OH stretch corresponds to ~13% higher E_{avail} (35% higher vibrational energy) than the OD stretch. In contrast, the analogous result for the NO_2H^+ channel (Figure 4, third frame) shows that the OH stretch causes larger attenuation than the OD stretch. At E_{col} = 0.76 eV, the products from the ground-state reaction can dissociate for v_{axial} inside of the pair of blue vertical lines, and the brown lines show the limits for the OH stretch excited reaction. The same mode-dependent attenuations are observed here.

It is useful to think about the OH versus OD stretch effects in terms of stretching the bond that breaks versus the spectator bond, that is, the bond in the OH or OD product. One might expect that energy initially deposited in the bond that breaks should be more efficiently channeled into the internal energy of the NO_2D^+ or NO_2H^+ product, while excitation in the spectator bond might tend to remain as vibrational excitation of the OH or OD product. The mode effects on the v_{axial} distributions show just this effect, as do the data in Figure 7. Note that for several E_{col} points, where E_{col} is well below the energy required for dissociation of the NO_2D^+ or NO_2H^+ products, the largest attenuation comes from OH stretch excitation, presumably because it can make the largest contribution to destabilizing the products. With increasing E_{col}, the attenuations become quite mode-dependent. For NO_2D^+, excitation of the OD stretch (bond that breaks) gives the largest attenuation, and excitation of the "spectator" OH stretch has a smaller effect, even though its energy is 35% greater. For NO_2H^+, the OD bond is the spectator, and as expected, exciting this stretch has a much smaller effect than exciting the OH stretch. In fact, at 1 eV and above, exciting the spectator stretch has no effect at all, whereas the stretch of the bond that breaks continues to destabilize the product.

The effect of bend excitation is less clear, partly because this is a significantly lower energy excitation and thus does not have a large effect on the energy available to destabilize the NO_2D^+ and NO_2H^+ products. In general, the bend causes a small suppression of the product signals, roughly in line with the effect that results from adding an equivalent amount of collision energy.

All HOD^+ modes inhibit CT (Figure 8, top) for E_{col} < 1 eV, with the largest effect from the bend, the lowest-frequency mode by a large margin. The large inhibition at low energies is partly due to the fact that survival of NO_2H^+ and NO_2D^+ is reduced by vibrational excitation, and secondary reaction of these product ions is a significant contributor to the NO_2^+ signal. As shown in Figure 7, the OH and OD stretch modes have the largest effect on NO_2H^+ and NO_2D^+ survival, and this secondary reaction probably explains the small inhibitory effect on the NO_2^+ cross section at low E_{col}. Note, however, that bend excitation, because its energy is low, has relatively little effect on NO_2H^+ and NO_2D^+ survival but has the largest effect on the NO_2^+ signal; thus, we conclude that bend excitation really does inhibit CT in this system. This conclusion is supported by the fact that at high E_{col}, where the secondary reaction contribution is negligible, the OH and OD stretch effects become negligible, but the bend continues to inhibit CT.

It is not clear why HOD^+ bend excitation might inhibit CT because there is little geometry change in the $HOD^+ \rightarrow HOD$ process and thus no reason to expect that the efficiency should depend on the bend angle. As noted, however, the total cross section is neither enhanced nor inhibited by bend excitation; thus, the effect may simply result from a bend enhancement of a competing channel. The only possibility for this role is the NO^+ production cross section, which is enhanced by bend excitation.

As discussed above, the NO^+ channel has potential contributions from up to five processes occurring on both singlet and triplet surfaces. It is inhibited by E_{col} and is the only channel enhanced by vibration. All three modes enhance NO^+ production, with the largest effect from the OH stretch and similar smaller effects from the bend and OD stretch modes. It is clear that a significant fraction of the enhancement, particularly that from OH and OD stretch excitation, results from the effects of stretching the "bond that breaks" upon the dissociation of NO_2H^+ and NO_2D^+ products

$$NO_2H^+ \rightarrow NO^+ + OH \qquad \text{and } NO_2D^+ \rightarrow NO^+ + OD$$

The effects at low E_{col}, where enough NO_2H^+ and NO_2D^+ survive to be detected, can be seen in Figure 7. Note that in the low E_{col} range, the bend has a smaller effect on NO_2H^+ and NO_2D^+ dissociation than either stretch, yet the enhancement in the NO^+ signal is comparable to that from the OD stretch. That indicates that there is a real enhancement in NO^+ production from HOD^+ bend excitation, beyond that from enhancing dissociation of NO_2H^+ and NO_2D^+. In this low-energy range, we believe that the other significant NO^+ production processes include triplet dissociative CT and possibly singlet HOOH elimination. It is not clear why bend excitation might enhance either of these reactions.

At high E_{col}, any NO_2H^+ or NO_2D^+ that is still formed is all dissociated to $NO^+ + OH$, regardless of HOD^+ vibrational excitation; thus, this NO^+ enhancement mechanism is no longer active. The fact that the effect of OD stretch excitation also dies out at high E_{col} suggests that this may have been the only enhancement mechanism for this mode. It is interesting that the OH stretch continues to enhance NO^+ production in the high E_{col} range, and this is also the only case where there is an enhancement of σ_{total}. We speculate that OH stretch excitation somehow enhances the probability of NO^+ production in grazing impact parameter collisions, such that the total cross section increases. The NO^+ production channels most likely to be enhanced at high E_{col} are dissociative CT on the singlet and triplet surfaces or formation and subsequent predissociation of triplet NO_2^+. The fact that the enhancement in σ_{total} appears starting at ~1 eV suggests that singlet dissociative CT is probably not responsible (threshold energy = 1.78 eV). The conclusion, then, is that some form of triplet dissociative CT is enhanced by OH stretch excitation.

IV. CONCLUSIONS

This is a complex reaction, with nine different channels on singlet and triplet surfaces resulting in five distinguishable products masses. Nonetheless, by comparing cross section magnitudes with the singlet and triplet collision cross sections, examining the recoil dynamics, and comparing to thermal energy kinetic measurements, we are able to largely sort out the branching between all of the pathways.

Because $NO^+ + HOOH$ production involves tight and high-energy transition states, we infer that it is probably a minor singlet channel. The dominant singlet channel is clearly CT, which may, in fact, account for nearly 100% of the branching on the singlet surface. There also may be some H^+ and D^+ transfer on the singlet surface; however, the reaction coordinate in Figure 1 suggests that these reactions probably mostly result from triplet coupled reactions. On the triplet surface, the dominant product channel is clearly NO^+ production, and it appears to have significant contributions from dissociative CT, predissociation of the triplet CT product ion, and dissociation of NO_2H^+ and NO_2D^+ products that have internal excitation above the threshold for OH/OD elimination.

HOD^+ vibrational excitation affects branching between the channels but has little effect on the overall reactivity, which is near the collision limit at the energies probed in the beam experiments. Vibrational energy put into the bond that breaks in H^+ or D^+ transfer is shown to end up as internal energy of the NO_2H^+ or NO_2D^+ product, whereas energy in the spectator bond does not, presumably indicating that energy remains in the OH or OD product.

Motivated by apparent problems with previous thermal kinetic measurements in the literature, we remeasured the thermal energy rates for this system. The results are consistent with the reaction coordinate in Figure 1. The main differences between the thermal and beam measurements are that long complex lifetimes on the triplet surface allow significant triplet → singlet conversion in the thermal measurements, whereas the collision times at beam energies are too short for significant triplet → singlet conversion. Furthermore, $NO^+(H_2O)$ is seen as a product in the thermal measurement, resulting from collisional stabilization of this complex in TC3. In the beam experiment, the internal energy of this complex is apparently always too high for it to survive without stabilizing collisions, and the product detected is NO^+. In addition, the thermal measurements do not see NO_2H^+ or NO_2D^+, presumably because collisions on the triplet surface that trap in the TC1 complex instead result in production of $NO^+(H_2O)$, while for the higher available energy range probed in the beam experiments, the higher-energy but more facile H^+/D^+ transfer reaction is significant.

AUTHOR INFORMATION

Corresponding Author
*E-mail: anderson@chem.utah.edu.

ACKNOWLEDGMENT

A.A.V. is grateful for the support of the Air Force Office of Scientific Research for this work. The Utah work is supported by a grant from the Chemistry Division of the National Science Foundation (CHE-0647124)

REFERENCES

(1) Bronikowski, M. J.; Simpson, W. R.; Girard, B.; Zare, R. N. *J. Chem. Phys.* **1991**, *95*, 8647.
(2) Bronikowski, M. J.; Simpson, W. R.; Zare, R. N. *J. Phys. Chem.* **1993**, *97*, 2204.
(3) Bronikowski, M. J.; Simpson, W. R.; Zare, R. N. *J. Phys. Chem.* **1993**, *97*, 2194.
(4) Sinha, A.; Hsiao, M. C.; Crim, F. F. *J. Chem. Phys.* **1990**, *92*, 6333.
(5) Sinha, A.; Thoemke, J. D.; Crim, F. F. *J. Chem. Phys.* **1992**, *96*, 372.
(6) Metz, R. B.; Thoemke, J. D.; Pfeiffer, J. M.; Crim, F. F. *J. Chem. Phys.* **1993**, *99*, 1744.
(7) Thoemke, J. D.; Pfeiffer, J. M.; Metz, R. B.; Crim, F. F. *J. Phys. Chem.* **1995**, *99*, 13748.
(8) Sinha, A.; Hsiao, M. C.; Crim, F. F. *J. Chem. Phys.* **1990**, *92*, 6333.
(9) Armentrout, P. B.; Simons, J. *J. Am. Chem. Soc.* **1992**, *114*, 8627.
(10) Dotan, I.; Lindinger, W.; Rowe, B.; Fahey, D. W.; Fehsenfeld, F. C.; Albritton, D. L. *Chem. Phys. Lett.* **1980**, *72*, 67.
(11) Shul, R. J.; Passarella, R.; DiFazio, L. T., Jr.; Keesee, R. G.; Castleman, A. W., Jr. *J. Phys. Chem.* **1988**, *92*, 4947.

(12) Chiu, Y.-H.; Fu, H.; Huang, J.-T.; Anderson, S. L. *J. Chem. Phys.* **1995**, *102*, 1188.
(13) Liu, J.; Kim, H.-T.; Anderson, S. L. *J. Chem. Phys.* **2001**, *114*, 9797.
(14) Uselman, B. W.; Boyle, J. M.; Anderson, S. L. *Chem. Phys. Lett.* **2007**, *440*, 171.
(15) *CRC Handbook of Chemistry and Physics*, 66 ed.; Weast, R. C., Astle, M., J., Beyer, W. H., Eds.; CRC Press: Boca Raton, FL, 1985.
(16) Ornellas, F. R.; Resendeb, S. M.; Machado, F. B. C.; Roberto-Neto, O. *J. Chem. Phys.* **2002**, *118*, 6.
(17) Viggiano, A. A.; Morris, R. A.; Dale, F.; Paulson, J. F.; Giles, K.; Smith, D.; Su, T. *J. Chem. Phys.* **1990**, *93*, 1149.
(18) Frisch, M. J.; Trucks, G. W.; Schlegel, H. B.; Scuseria, G. E.; Robb, M. A.; Cheeseman, J. R.; J. A. Montgomery, J.; Vreven, T.; Kudin, K. N.; Burant, J. C.; Millam, J. M.; Iyengar, S. S.; Tomasi, J.; Barone, V.; Mennucci, B.; Cossi, M.; Scalmani, G.; Rega, N.; Petersson, G. A.; Nakatsuji, H.; Hada, M.; Ehara, M.; Toyota, K.; Fukuda, R.; Hasegawa, J.; Ishida, M.; Nakajima, T.; Honda, Y.; Kitao, O.; ; Nakai, H.; Klene, M.; Li, X.; Knox, J. E.; Hratchian, H. P.; Cross, J. B.; Adamo, C.; Jaramillo, J.; Gomperts, R.; Stratmann, R. E.; Yazyev, O.; Austin, A. J.; Cammi, R.; Pomelli, C.; Ochterski, J. W.; Ayala, P. Y.; Morokuma, K.; Voth, G. A.; Salvador, P.; Dannenberg, J. J.; Zakrzewski, V. G.; Dapprich, S.; Daniels, A. D.; Strain, M. C.; Farkas, O.; Malick, D. K.; Rabuck, A. D.; Raghavachari, K.; Foresman, J. B.; Ortiz, J. V.; Cui, Q.; Baboul, A. G.; Clifford, S.; Cioslowski, J.; Stefanov, B. B.; Liu, G.; Liashenko, A.; Piskorz, P.; Komaromi, I.; Martin, R. L.; Fox, D. J.; Keith, T.; Al-Laham, M. A.; Peng, C. Y.; Nanayakkara, A.; Challacombe, M.; Gill, P. M. W.; Johnson, B.; Chen, W.; Wong, M. W.; Gonzalez, C.; Pople, J. A. *Gaussian 03*, revision B.02; Gaussian, Inc.: Pittsburgh PA, 2003.
(19) Hase, W. L.; Bolton, K.; de Sainte Claire, P.; Duchovic, R. J.; Hu, X.; Komornicki, A.; Li, G.; Lim, K.; Lu, D.; Peslherbe, G. H.; Song, K.; Swamy, K. N.; Vande Linde, S. R.; Varandas, A.; Wang, H.; Wolf, R. J. *VENUS99: A general chemical dynamics computer program*, Wayne State University: Detroit, MI, 1999.
(20) Bakken, V.; Millam, J. M.; Schlegel, H. B. *J. Chem. Phys.* **1999**, *111*, 8773.
(21) Shibuya, K.; Suzuki, S.; Imamura, T.; Koyano, I. *J. Phys. Chem. A* **1997**, *101*, 685.
(22) Hunter, E. P.; Lias, S. G. *J. Phys. Chem. Ref. Data* **1998**, *27*, 413.
(23) Ruscic, B.; Morton, M. L.; Pinzon, R. E.; Laszewski, G. v.; Bittner, S.; Nijsure, S. G.; Amin, K. A.; Minkoff, M.; Wagner, A. F. *J. Phys. Chem. A* **2004**, *108*, 9979.
(24) Ruscic, B.; Pinzon, R. E.; Morton, M. L.; Srinivasan, N. K.; Su, M.-C.; Sutherland, J. W.; Michael, J. V. *J. Phys. Chem. A* **2006**, *110*, 6592.
(25) Scott, A. P.; Radom, L. *J. Phys. Chem.* **1996**, *100*, 16502.
(26) Afeefy, H. Y.; Liebman, J. F.; Stein, S. E. Neutral Thermochemical Data. In *NIST Chemistry WebBook, NIST Standard Reference Database Number 69*; Mallard, W. G., Linstrom, P. J., Eds.; National Institute of Standards and Technology: Gaithersburg, MD, 2000; http://webbook.nist.gov.
(27) Lias, S. G.; Bartmess, J. E.; Liebman, J. F.; Holmes, J. L.; Levin, R. D.; Mallard, W. G. Ion Energetics Data. In *NIST Chemistry WebBook, NIST Standard Reference Database Number 69*; Mallard, W. G., Linstrom, P. J., Eds.; National Institute of Standards and Technology: Gaithersburg, MD, 2000; http://webbook.nist.gov.
(28) Fehsenfeld, F. C.; Howard, C. J.; Schmeltekopf, A. L. *J. Chem. Phys.* **1975**, *63*, 2835.
(29) Anicich, V. G. *An Index of the Literature for Bimolecular Gas Phase Cation-Molecule Reaction Kinetics*; National Aeronautics and Space Administration, and Jet Propulsion Laboratory,California Institute of Technology: Pasadena, CA, 2003.
(30) Viggiano, A. A.; Arnold, S. T.; Morris., R. A. *Int. Rev. Phys. Chem.* **1998**, *17*, 147.
(31) Zhu, L.; Hase, W. L. *A general RRKM Program; Quant. Chem. Prog. Exchange, QCPE*; Chemistry Department: University of Indiana, 1993; p 644.
(32) Troe, J. *Chem. Phys. Lett.* **1985**, *122*, 425.
(33) Levine, R. D.; Bernstein, R. B. *Molecular Reaction Dynamics and Chemical Reactivity*; Oxford University Press: New York, 1987.
(34) Ramsey, N. F. *Molecular Beams*; Oxford University Press: New York, 1956.
(35) Chiu, Y.-H.; Fu, H.; Huang, J.-T.; Anderson, S. L. *J. Chem. Phys.* **1995**, *102*, 1199.
(36) Chiu, Y.-H.; Fu, H.; Huang, J.-T.; Anderson, S. L. *J. Chem. Phys.* **1996**, *105*, 3089.
(37) Qian, J.; Fu, H.; Anderson, S. L. *J. Phys. Chem.* **1997**, *101*, 6504.
(38) Liu, J.; Van Devener, B.; Anderson, S. L. *J. Chem. Phys.* **2004**, *121*, 11746.
(39) Liu, J.; Uselman, B.; Van Devener, B.; Anderson, S. L. *J. Phys. Chem. A* **2004**, *108*, 9945.
(40) Honma, K.; Armentrout, P. B. *J. Chem. Phys.* **2004**, *121*, 8307.
(41) Kimura, K.; Katsumata, S.; Achiba, Y.; Yamazaki, T.; Iwata, S. *Handbook of HeI Photoelectron Spectra of Fundamental Organic Molecules*; Japan Scientific Societies Press: Tokyo, 1981.
(42) Baltzer, P.; Karlsson, L.; Wannberg, B.; Holland, D. M. P.; MacDonald, M. A.; Hayes, M. A.; Eland, J. H. D. *Chem. Phys.* **1998**, *237*, 451.